Beamforming Orthogonality in Coupled Directional Modulation Arrays

Beamforming Orthogonality in Coupled Directional Modulation Arrays

Jiayu Hou[1, 2], Haijun Fan[1], Yuan Ding[1], Yue Xiao[3], Symon Podilchak[2]
[1] Institute of Sensors, Signals and Systems, Heriot-Watt University, Edinburgh, UK, {jh2064; h.fan; yuan.ding}@hw.ac.uk
[2] Institute of Digital Communications, University of Edinburgh, Edinburgh, UK, s.podilchak@ed.ac.uk
[3] National Key Laboratory of Science and Technology on Communications, University of Electronic Science and Technology of China, Chengdu, China, xiaoyue@uestc.edu.cn

***Abstract*— This paper studies the orthogonality in a directional modulation (DM) transmitter equipped with an antenna array whose mutual coupling is considered. The antenna coupling will generate backward waves at the power amplifier (PA) outputs. This dynamic interaction will drive the PA load away from the system characteristic impedance thus introducing the loadpulling effect to the system which would result in the distortion to the DM system orthogonality. When the antenna coupling is considered, for a certain target user, the leakage radiation from the information beams designed for other users and from the generated artificial noise would become the interference to this user, and in one example given in this paper, the signal to interference ratios (SIR) of around 20 dB are observed. This compromise of the DM orthogonality would put a performance upper limit to a DM system considering a coupled antenna array.**

***Index Terms*— antenna coupling, directional modulation (DM), orthogonality, power amplifier (PA) loadpulling, signal to interference ratio (SIR).**

I. INTRODUCTION

Directional modulation (DM), a keyless physical-layer wireless security technology, is receiving significant attention in recent years [1], [2]. It has the capability of confining the spatial region, or in free space narrowing the angular sector, within which the information bearing signals can be correctly retrieved. DM transmitters can take many forms, such as arrays consisting of coupled parasitic [3] or reconfigurable radiating elements [4], and phased [5] or lens [6] arrays. Though different architecture, their underlying principle was similar, which was revealed using orthogonal vector concept in [7] for single user, and in [8], [9] for multi-user. Since then, more DM research efforts have been made in, e.g., improving energy efficiency [10]–[13] reducing complexity [14], [15] and its linearization [16].

It has been understood that DM functionality is achieved through orthogonality between information beams and artificial noise beams along the desired direction for a single user scenario [17], or, orthogonality between the information beam for one user and other information beams for the remaining users (and possibly extra artificial noise) for a multi-user scenario [18]. However, most DM works reported previously are based on the assumption of an uncoupled antenna array with isotropic active element radiation patterns, as well as identical and linear power amplifiers (PAs) connected at each antenna branch. In practice, consecutive antenna elements in an array are separated with a half wavelength (denoted as $\lambda/2$), which, unfortunately, still contributes to non-negligible mutual coupling levels. Moreover, when PAs are exposed to those coupled antennas, their load impedance would be actively pulled, involving loadpulling effects [19]. This nonlinear interaction between the PAs and the antenna array will unfortunately generate interference and compromise orthogonality that is required in various DM systems. This phenomenon is studied in this work for both single-user and multi-user scenarios.

In this paper, we will point out that the PA nonlinearity caused by antenna mutual coupling and the subsequent loadpulling effect will compromise the orthogonality between the secure information transmission and the artificial noise generated by the conventional DM transmitters designed using orthogonal vector approach [7], [8]. The structure of a DM transmitter, and the interaction between PAs and coupled antenna arrays will be explained in Section II, which is followed by performance simulations for both single-user and multi-user DM systems using an example of a 7-element linear DM array. This is explored in Section III. The performance drop caused by the PAs and coupled antenna array interaction is also examined in this section. Finally, Section IV concludes this paper and provides future research directions.

In this paper, bold letter refers to a row vector. $(\cdot)^{-1}$ and $(\cdot)^{\dagger}$ denote operators for pseudo inverse and Hermitian conjugate, respectively. Operator $\|\cdot\|$ returns the norm of the enclosed vector. $[\cdot]$ represents a matrix. $[\boldsymbol{I}_N]$ is the $N\times N$ identical matrix.

II. SYSTEM MODEL

A DM transmitter consisting of an N-element linear active antenna array, as studied in this paper, is shown in Fig. 1. In each branch a PA is connected with the associated antenna element. It is well known that PA characteristics are very much dependent on its load reflection coefficient Γ_n (n = 1, 2, …, N), which is defined by the ratio between the backward wave a_n and forward wave b_n, labelled in Fig. 1. The PA output load impedance Z_n can be calculated from Γ_n using (1), where Z_0 is system characteristic impedance, 50 Ω in most systems and also in our study.

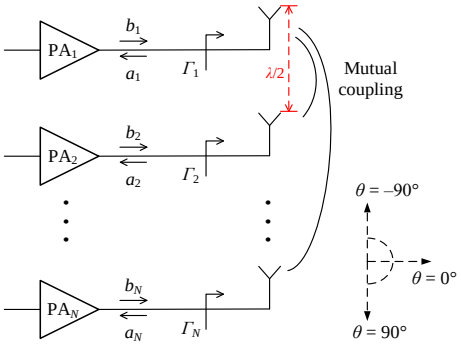

Fig. 1. A DM transmiter with N-element linear antenna array.

$$Z_n = Z_0 \frac{1+\Gamma_n}{1-\Gamma_n} \tag{1}$$

In all the following discussions, it is assumed that the PA input port is perfectly matched. In most reported DM works no antenna mutual coupling is considered, i.e., all antenna elements are well-matched with $a_n = 0$, thus $\Gamma_n = 0$, and $Z_n = Z_0$. Based on the orthogonal vector DM synthesis approach proposed in [7], [8], an excitation vector $\boldsymbol{E}_i$ for an i^{th} symbol in a DM transmitter can be synthesized using

$$\boldsymbol{E}_i = \left(\sum_{k=1}^{K} A_{ik} \boldsymbol{\Lambda}_k \right) + \boldsymbol{W}_{ov\_i}, \tag{2}$$

where A_{ik} is the i^{th} symbol, i.e., the complex number in IQ plane, to be conveyed for the k^{th} legitimate user along the k^{th} desired secure communication direction (k = 1, 2, …, K, and $K < N$). The vector $\boldsymbol{\Lambda}_k$, defined in (3), for each k is orthogonal to the channels associated with all the other users, i.e., $\boldsymbol{H}_m^{\dagger} \boldsymbol{\Lambda}_k = 0$ for $m \neq k$. Here the n^{th} element in the column vector $\boldsymbol{H}_m$ is the channel coefficient between the n^{th} antenna element to the m^{th} user. The vector $\boldsymbol{W}_{ov\_i}$ is the orthogonal vector, named as orthogonal artificial noise in some other works, which is updated in the null space of the channel matrix [$\boldsymbol{H}$] whose columns are vectors $\boldsymbol{H}_k$ for k = 1, 2, …, K. In an ideal non-coupled DM array, this $\boldsymbol{E}_i$ can be regarded identically as the inputs of the PA array (assuming they operate in linear region) or as the inputs of the antenna array. The linear PA gain is normalized out in the study, since it does not affect the DM orthogonality. This is not the case in practice when the antenna coupling exists.

$$\boldsymbol{\Lambda}_k = \frac{1}{\left\| \boldsymbol{H}_k \right\|^2} \left(\prod_{m=1, m\neq k}^{K} \left([\boldsymbol{I}_N] - \boldsymbol{H}_m^{-1} \boldsymbol{H}_m^{\dagger} \right) \right) \boldsymbol{H}_k \tag{3}$$

However, coupling among antenna elements is inevitable, i.e., $a_n \neq 0$. Thus, from (1) we know that the PA load impedance is no longer 50 Ω, and this impedance is dependent on the dynamic signals transmitted by all coupled antennas.

As an example, Fig. 2 shows the simulated PA loadpull contours for gain and output power at 1 dB compression point (P_{1dB}). Here Indium Gallium Phosphide PA GVA-63+ from

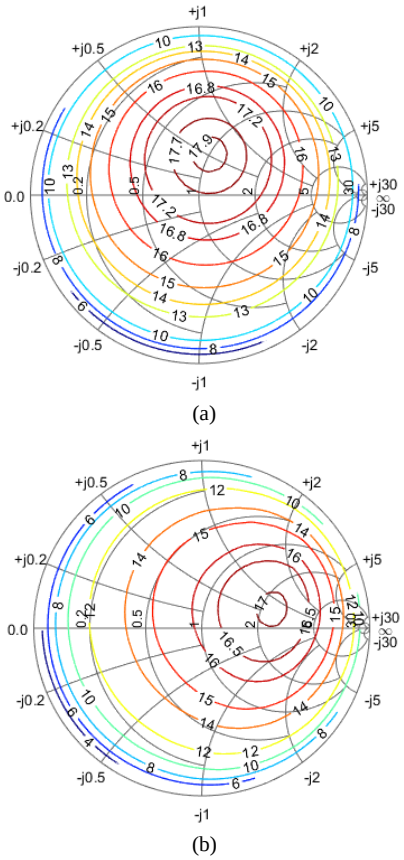

Fig. 2. Simulated PA GVA-63+ loadpull contours for (a) gain and (b) output power at P_{1dB}, plotting on 50 Ω normalized Smith charts.

Mini-Circuits is used. It can be clearly seen that when PA loads deviates from 50 Ω (the center on the Smith chart), its characteristics, like gain, output power, efficiency, and non-linearity, are different. It is expected that this dynamic PA load variation, as a result of antenna coupling and PA loadpulling effect, will compromise the orthogonality in DM systems, as guaranteed by (3) in non-coupled ideal DM transmitters. This aspect will be studied in the next section using an example.

III. Impact of Antenna Coupling and PA Loadpulling on DM Orthogonality

In this section, as an example, an N = 7 element linear patch antenna array operating at 3.5 GHz, seen in Fig. 3, is used to construct a DM transmitter. Each antenna is capacitively fed, see the inset. They are simulated in the full-wave electromagnetic simulation software CST, and the individual radiation patterns in the x-z plane are plotted in Fig. 4. Fig. 4 shows that the active element patterns for each antenna are different, and overall they have a broad beam covering –50° to 50° with 0° along the array boresight.

The simulated S-matrix of the array at 3.5 GHz are listed in Table I. It can be seen that each antenna is well matched (all below –20 dB in the diagonal), and the strongest coupling between adjacent elements is about –15 dB.

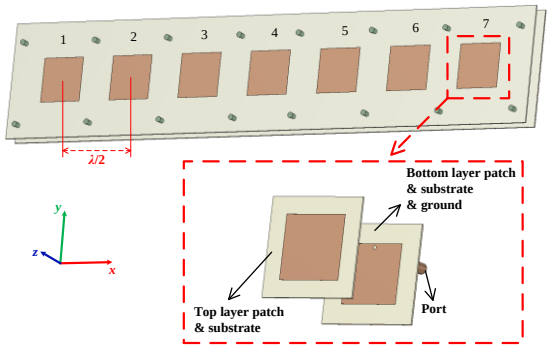

Fig. 3. 1-by-7 linear patch antenna array, operating at 3.5 GHz, designed in CST for our study in this paper.

When importing the array S-matrix into ADS, with the availability of the PA GVA-63+ model (input and output matched to 50 Ω), the PA output impedance can be obtained using harmonic balance simulation for a given excitation $\boldsymbol{E}_i$ at the PA inputs. Here the subscript 'i' refers to the time slot for the i^{th} symbol. For simplicity it is omitted hereafter. It is noted that the excitation is given a well back off, ensuring all PAs operate in linear region, so that the orthogonality reduction among vectors $\boldsymbol{\Lambda}_k$ and $\boldsymbol{W}_{ov}$ we will show later on is purely caused by active loadpulling effect. When no coupling is considered, all PAs operate in the same condition, so the PAs output vector (or equivalently the array input vector) is the same as the PAs input vector $\boldsymbol{E}$ subject to a gain scaling. In a more practical condition where the antenna coupling exists, each PA will operate in different conditions because of the active loadpulling effect, see the simulated results in Table II. It can be seen from the last row in Table II that the gains are different for different PAs. As a further explanation of this non-identical amplification, the PA loads, scattering on the Smith chart, are presented in Fig. 5 associated with the scenarios in Table II. Under the same condition, the AM/AM curves are given in Fig. 6 for the PA GVA-63+ under the loads Z_2 and Z_5 (shown in Fig. 5, and for Table II).

The gain G_n for each PA can be obtained by comparing PA input $\boldsymbol{E}$ and PA output $\boldsymbol{F}$ in Table II. It is known from (2) that the excitation $\boldsymbol{E}$ is a comprise of $\boldsymbol{\Lambda}_k$ and $\boldsymbol{W}_{ov}$, thus similarly the output $\boldsymbol{F}$ consists of amplified $\boldsymbol{\Lambda}_k$ and $\boldsymbol{W}_{ov}$. Normalizing PA outputs of both systems with the PA gain under 50 Ω, the non-coupled system will get the PA input excitation $\boldsymbol{E}$ while the coupled DM system will get its distorted counterpart $\boldsymbol{E}'$,

TABLE I. SIMULATED S-MATRIX OF THE ANTENNA ARRAY IN FIG. 3 FOR 3.5 GHZ ~~OPEARTION~~OPERATION.

S_{ij} (dB∠°)	j = 1	j = 2	j = 3	j = 4	j = 5	j = 6	j = 7
i = 1	−20.3∠−154°	−16.0∠−55°	−22.9∠129°	−29.0∠−44°	−36.2∠142°	−50.2∠−34°	−45.9∠−48°
i = 2	−15.9∠−55°	−21.6∠−177°	−15.1∠−60°	−21.7∠121°	−27.4∠−55°	−34.3∠128°	−49.9∠−34°
i = 3	−22.7∠132°	−15.1∠−60°	−21.8∠173°	−14.8∠−62°	−21.3∠120°	−27.3∠−55°	−36.0∠−142°
i = 4	−28.5∠−38°	−21.6∠121°	−14.8∠−62°	−21.7∠171°	−14.8∠−62°	−21.6∠−121°	−28.9∠−44°
i = 5	−35 .2∠154°	−27.3∠−55°	−21.3∠−120°	−14.8∠−62°	−21.8∠173°	−15.1∠−60°	−22.9∠−128°
i = 6	−47.2∠7°	−34.3∠128°	−27.4∠−55°	−21.7∠121°	−15.1∠−60°	−21.6∠−178°	−15.6∠−55°
i = 7	−44.0∠−61°	−50.2∠−34°	−36.2∠141°	−29.0∠−44°	−22.9∠129°	−16.0∠−55°	−20.4∠−154°

TABLE II. SIMULATED PA OUTPUT VECTOR $\boldsymbol{F}$ FOR A GIVEN PA INPUT $\boldsymbol{E}$ WHEN THE ANTENNA COUPLING SHOWN IN TABLE I IS CONSIDERED. IN THIS EXAMPLE, K = 1, A_k = 1, θ_1 = 0°. $(\cdot)_n$ REFERS TO THE n^{th} ELEMENT IN ENCLOSED VECTOR. (THE SUBSCRIPT i IS OMMITED.)

dB∠°	n = 1	n = 2	n = 3	n = 4	n = 5	n = 6	n = 7
Λ_{1n}	−28.7∠58°	−30.3∠60°	−29.2∠−59°	−30.2∠−59°	−29.2∠−59°	−30.3∠−60°	−28.7∠−58°
W_{ov_n}	−29.2∠−153°	−40.6∠163°	−22.1∠2°	−40.5∠164°	−39.5∠164°	−40.6∠163°	−39.0∠165°
E_n	−26.4∠−104°	−32.2∠−75°	−20∠−15°	−32.1∠−74°	−31.1∠−74°	−32.2∠−75°	−30.6∠−73°
F_n	−8.4∠84°	−11.2∠114°	−2.7∠179°	−10.8∠117°	−13.3∠101°	−12.9∠113°	−12.5∠114°
$G_n = F_n/E_n$	18.0∠−172°	21.0∠−171°	17.3∠−166°	21.3∠−169°	17.8∠175°	19.3∠−172°	18.1∠−173°

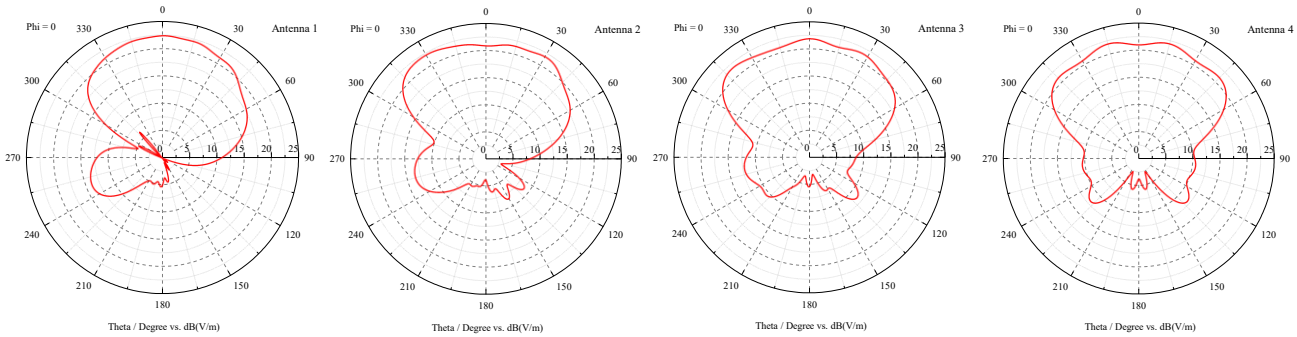

Fig. 4. CST simulated radiation patterns in x-z plane for antennas 1 to 4 (see indices in Fig. 3). Patterns of antennas 5 to 7 are mirror symmetric to antennas 3 to 1, thus they are omitted.

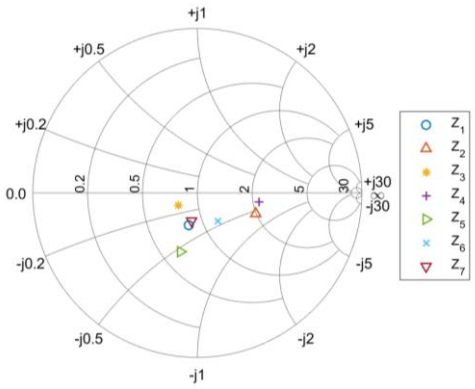

Fig. 5. Simulated 7 PA load impedance Z_n (or equivalently coupled antenna impedance), plotting on 50 Ω normalized Smith charts for the operating scenario in Table II.

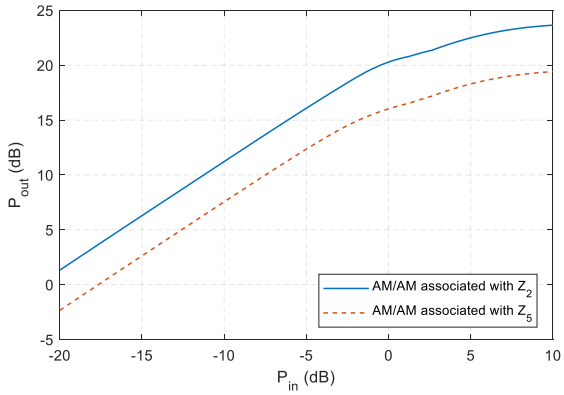

Fig. 6. Simulated AM/AM curves for the PA under loads Z_2 and Z_5 labelled in Fig. 5.

which is the sum of distorted signal vector $\boldsymbol{\Lambda}_k'$ and noise vector $\boldsymbol{W}_{ov}'$. The radiation patterns associated with the example $\boldsymbol{\Lambda}_1$ and $\boldsymbol{W}_1$ in Table II for the ideal non-coupled DM array is plotted in Fig. 7(a). It is clear that the generated information pattern and artificial noise pattern are orthogonal along the desired secure communication direction $\theta_1 = 0°$. This is expected because the orthogonality is guaranteed by (3) and the fact that $\boldsymbol{W}_{ov}$ is in the null space of $[\boldsymbol{H}]$. When antenna coupling and PA loadpulling effect is considered, the patterns associated with $\boldsymbol{\Lambda}_k'$ and $\boldsymbol{W}_{ov}'$ are also plotted in Fig. 7(a) for comparison. The orthogonality between the information beam and the artificial noise beam is clearly compromised, resulting in a signal to interference ratio (SIR) of around 20 dB. This is also true for other selected secure communication directions, such as the one along 20° depicted in Fig. 7(b).

Through the two plots in Fig. 7, it is found that within the main beam, the gain is 1 to 2 dB deviating around that of a perfectly isolated array. In these two simulation examples, the DM power efficiency PE_{DM}, defined in [20], is set to 0.5. When more than one user needs to be served by the DM array, the impact of antenna coupling and PA loadpulling will be more severe, see an example for a two-user case in Fig. 8. It is assumed that these two users are located along $\theta_1 = -30°$ and $\theta_2 = 10°$. Similar to the single-user case, the orthogonality among information beams along θ_1 and θ_2, as well as the artificial noise radiation, is no longer held in the coupled DM array. The SIR for the user along the direction θ_1 reduces to about 17 dB; for the other user the SIR is dropped to roughly 22 dB. It is foreseen that the increase of the number of users and the coupling among array antennas will further deteriorate the DM orthogonality.

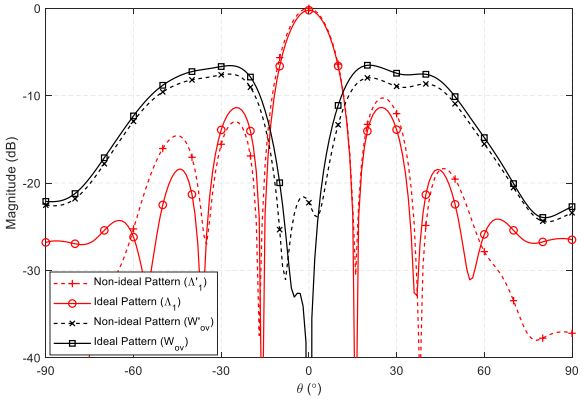

(a)

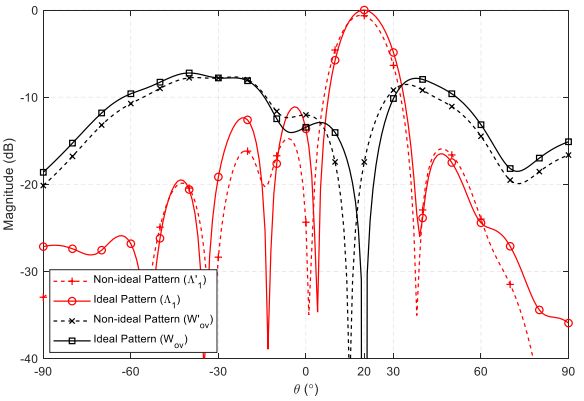

(b)

Fig. 7. Simulated radiation patterns, with the maximun magnitude normalized to 0 dB, associated with excitations $\boldsymbol{\Lambda}_1$ and $\boldsymbol{W}_{ov}$ for ideal DM array and associated with excitations $\boldsymbol{\Lambda}_1'$ and $\boldsymbol{W}_{ov}'$ for non-ideal coupled DM array. $PE_{DM} = 0.5$. (a) $\theta_1 = 0°$, (b) $\theta_1 = 20°$.

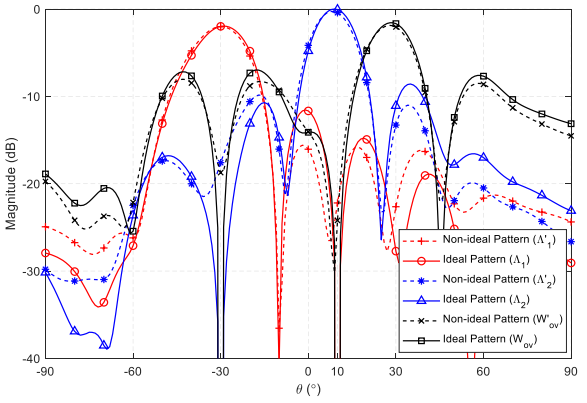

Fig. 8. Simulated radiation patterns with the maximun magnitude normalized to 0 dB, associated with excitations $\boldsymbol{\Lambda}_1$, $\boldsymbol{\Lambda}_2$, and $\boldsymbol{W}_{ov}$ for ideal DM array and associated with excitations $\boldsymbol{\Lambda}_1'$, $\boldsymbol{\Lambda}_2'$, and $\boldsymbol{W}_{ov}'$ for non-ideal coupled DM array. $\theta_1 = -30°$ and $\theta_2 = 10°$.

IV. Conclusion

This work studied the orthogonality in DM transmitters with coupled antenna array elements. When the mutual coupling was considered, the PA loadpulling effect occurred, and it brought an extra source of nonlinearity, which would compromize the DM system orthogonality. Observed from the studied example that even when the PAs operated in a linear region, the dynamic loads would cause distortion to the excitation vectors, and this caused interference leakage along the desired secure communication directions. In this example, about 20 dB SIR was experienced in the coupled DM array.

Because of the non-uniform gain of the PAs in the transmitter array, the desired transmission signals will suffer from extra interference. As a result, the link performance would also drop. Potential solutions, designing PA resilient to the load variation, or developing constant envelope signal generation methods can be extended to multi-user and multi-carrier scenarios, will be explored in our future work. In other perspectives, utilizing the PA loadpulling effect to generate power efficient artificial noise can be another research direction.

Acknowledgment

This work was supported by UK Engineering and Physical Sciences Research Council under the Grant EP/V002635/1. The authors are grateful to Modelithics for the donation of software component model libraries to Heriot-Watt University under the Modelithics University Program.

References

[1] J. M. Purushothama, J. Hou, Y. Ding, and Y. Xiao, Radio frequency informed physical layer security – An augmented padlock to wireless transmission secrecy, book chapter for IET Book 'Physical Layer Security for 6G Networks', in press, 2023.

[2] F. Shu, et al., "Directional modulation: A physical-layer security solution to B5G and future wireless networks," *IEEE Network*, vol. 34, no. 2, pp. 210–216, March/April 2020.

[3] A. Babakhani, D. B. Rutledge, and A. Hajimiri, "Near-field direct antenna modulation," *IEEE Microw. Mag.*, vol. 10, no. 1, pp. 36–46, Feb. 2009.

[4] M. P. Daly and J. T. Bernhard, "Beamsteering in pattern reconfigurable arrays using directional modulation," *IEEE Trans. Antennas Propag.*, vol. 58, no. 7, pp. 2259–2265, Jul. 2010.

[5] M. P. Daly and J. T. Bernhard, "Directional modulation technique for phased arrays," *IEEE Trans. Antennas Propag.*, vol. 57, no. 9, pp. 2633–2640, Sep. 2009.

[6] Y. Ding, Y. Zhang, and V. Fusco, "Fourier Rotman lens enabled directional modulation transmitter," *Int. J. Antennas Propag.*, vol. 2015, Apr. 2015.

[7] Y. Ding and V. Fusco, "A vector approach for the analysis and synthesis of directional modulation transmitters," *IEEE Trans. Antennas Propag*, vol. 62, no. 1, pp. 361–370, Jan. 2014.

[8] Y. Ding and V. Fusco, "Orthogonal vector approach for synthesis of multi-beam directional modulation transmitters," *IEEE Antennas Wireless Propag. Lett.*, vol. 14, pp. 1330–1333, Feb. 2015

[9] F. Shu, X. Wu, J. Li, R. Chen, and B. Vucetic, "Robust synthesis scheme for secure multi-beam directional modulation in broadcasting systems," *IEEE Access*, vol. 4, pp. 6614–6623, Oct. 2016.

[10] J. M. Purushothama, Y. Ding, G. Goussetis, G. Huang, and Y. Xiao, "Synthesis of energy efficiency-enhanced directional modulation transmitters", *IEEE Trans. Green Commun. Netw.*, vol.7, no.2, pp.635–648, Sep. 2023.

[11] L. Chen, W. Chen, Y. Liu, C. Yang, and Z. Feng, "An efficient directional modulation transmitter with novel crest factor reduction technique", *IEEE Microw. Wireless Compon. Lett.*, vol. 29, no. 8, pp. 554–556, Aug. 2019.

[12] J. Hou, J. M. Purushothama, H. Fan, C. Song, Y. Ding, and M. Sellathurai, "Energy efficient time-modulated OFDM directional modulation transmitters," *Microw. Opt. Technol. Lett.*, vol. 65, no. 1 pp. 5–13, Jan. 2023.

[13] B. Zhang, W. Liu, and Q. Li, "Multi-carrier waveform design for directional modulation under peak to average power ratio constraint," *IEEE Access*, vol. 7, pp. 37528–37535, Mar. 2019.

[14] B. Zhang, W. Liu, and X. Lan, "Directional modulation design based on crossed-dipole arrays for two signals with orthogonal polarisations," in *Proc. Eur. Conf. Antennas Propag.*, London, UK, pp. 1–5, Apr. 2018.

[15] A. Narbudowicz, A. Zandamela, N. Marchetti and M. J. Ammann, "Energy-efficient dynamic directional modulation with electrically small antennas", *IEEE Antennas Wireless Propag. Lett.*, vol. 21, pp. 681–684, 2022.

[16] L. Chen, et al., "Linearization of a Directional Modulation Transmitter Using Low-Complexity Cascaded Digital Predistortion," *IEEE Trans. Microw. Theory Techn.*, vol. 67, no. 11, pp. 4467–4478, Nov. 2019.

[17] Y. Ding and V. Fusco, "Directional modulation far-field pattern separation synthesis approach," *IET Microw., Antennas Propag.*, vol. 9, no. 1, pp. 41–48, Jan. 2015.

[18] Y. Ding and V. Fusco, "MIMO Inspired synthesis of directional modulation systems," *IEEE Antennas Wireless Propag. Lett.*, vol. 15, pp. 580–584, Jul. 2015.

[19] H. Fan, Y. Ding, G. Goussetis, and M. J. Canavate Sanchez, "Antenna array driven by non-isolated power amplifiers for MIMO applications," in *49th Eur. Microw. Conf.*, Paris, France, Nov. 2019, pp. 468–471.

[20] Y. Ding and V. Fusco, "Establishing metrics for assessing the performance of directional modulation systems," *IEEE Trans. Antennas Propag.*, vol. 62, no. 5, pp. 2745–2755, Feb. 2014.